JoT JOURNAL OF TURBULENCE

http://jot.iop.org/

A dilating vortex particle method for compressible flow*

Jeff D Eldredge†, Tim Colonius and Anthony Leonard

California Institute of Technology, Pasadena, CA 91125, USA
E-mail: jde26@eng.cam.ac.uk

Received 20 September 2002
Published 9 October 2002

Abstract. Vortex methods have become useful tools for the computation of incompressible fluid flow. In this work, a vortex particle method for the simulation of unsteady two-dimensional compressible flow is developed. By decomposing the velocity into irrotational and solenoidal parts, and using particles that are able to change volume and that carry vorticity, dilatation, enthalpy, entropy and density, the equations of motion are satisfied. Spatial derivatives are treated using the method of particle strength exchange with high-order-accurate, non-dissipative kernels. The new vortex method is applied to co-rotating and leapfrogging vortices in compressible flow, with the far acoustic field computed using a two-dimensional Kirchhoff surface.

PACS numbers: 47.32.Cc, 02.70.Ns, 47.40.Dc, 47.27.Sd

Contents

* This article was chosen from Selected Proceedings of the 4th International Workshop on Vortex Flows and Related Numerical Methods (UC Santa-Barbara, 17–20 March 2002) ed E Meiburg, G H Cottet, A Ghoniem and P Koumoutsakos.

† Present address: Department of Engineering, Cambridge University, Cambridge CB2 1PZ, UK.

 PII: S1468-5248(02)53975-8 1468-5248/02/000001+10$30.00

JoT 3 (2002) 036

1. Introduction

Significant development in the past three decades has made vortex particle methods an attractive alternative to traditional fixed-grid computational schemes such as finite difference and finite volume methods [1]. The goal of the this work is to extend vortex methods, while retaining as many of their desirable properties as possible, to compressible flows, including those involving sound generation.

Techniques for accounting for compressibility effects have been included in particle methods previously, some of which are evident in the method presented here. The method of smoothed particle hydrodynamics (SPH) [2] and the transport-element method [3, 4] incorporate compressibility to a limited degree. In [5] fluid dilatation behind the flame front is accounted for in the velocity field by using regularized volume sources collocated with the vortex particles, a technique that will be employed in this paper. Quackenbush *et al* [6] developed a vortex method in which the density and reacting components are transported by the particles along with the vorticity. The particle volumes are allowed to change to conserve mass, a crucial element of the present method. By assuming low Mach number, they allow the density to only change with temperature, thus simplifying the particle equations.

The importance of vorticity in sound generation has been established by many investigators through the development of acoustic analogies valid for low Mach number flow (e.g., [7]). Previous investigations of sound generation using vortex methods [8, 9] have relied on low Mach number to use these acoustic analogies with an incompressible simulation of the near field. A numerical method which emphasizes the motion of vorticity in a compressible medium without the aid of a low-Mach-number assumption can be used to further explore, and possibly exploit, the relationship between vorticity and sound for more general flows. In the present method we will solve the full equations of compressible flow.

The goal of this investigation is the simultaneous solution of the near-field dynamics and a portion of the far-field sound by a homogeneous particle method. Inevitably some of the strength of vortex methods is compromised when applied to general compressible flows. Because the computational elements will carry radiating quantities in addition to vorticity, the region that they fill will necessarily be larger. Furthermore, such a method will require more delicate application of techniques that have proven robust in previous methods. In section 2 we develop the method, using particle strength exchange (PSE) for spatial derivatives. In section 3 the characteristics of PSE in the context of wave propagation are explored. Results from the simulation of co-rotating and leapfrogging vortices are shown and discussed in section 4.

2. Methodology

The velocity field is decomposed into solenoidal and irrotational components, $\boldsymbol{u} = \boldsymbol{u}_s + \boldsymbol{u}_{ir}$, where $\boldsymbol{u}_s \equiv \nabla \times \boldsymbol{A}$, $\boldsymbol{u}_{ir} \equiv \nabla\varphi$ and $\boldsymbol{A}$ is chosen to be solenoidal. Thus $\nabla^2\boldsymbol{A} = -\nabla \times \boldsymbol{u} \equiv -\boldsymbol{\omega}$ and $\nabla^2\varphi = \nabla \cdot \boldsymbol{u} \equiv \theta$. These equations are inverted using the Green function for the negative Laplacian G and the resulting velocity field is $\boldsymbol{u} = (\boldsymbol{K}\times) \star \boldsymbol{\omega} - \boldsymbol{K} \star \theta$, where $\boldsymbol{K} \equiv \nabla G$. The first term is the Biot–Savart integral, and the second is its dilatational counterpart.

The vorticity and dilatation fields are approximated by regularized particles,

$$\widetilde{\boldsymbol{\omega}}(\boldsymbol{x}, t) = \sum_p \boldsymbol{\Gamma}_p(t)\zeta_\varepsilon(\boldsymbol{x} - \boldsymbol{x}_p(t)), \qquad \widetilde{\theta}(\boldsymbol{x}, t) = \sum_p Q_p(t)\zeta_\varepsilon(\boldsymbol{x} - \boldsymbol{x}_p(t)), \tag{1}$$

where $\boldsymbol{\Gamma}_p = V_p\boldsymbol{\omega}(\boldsymbol{x}_p)$ and $Q_p = V_p\theta(\boldsymbol{x}_p)$. The function ζ_ε is the blob function scaled by ε, the radius of the blob—$\zeta_\varepsilon(\boldsymbol{x}) = \zeta(\boldsymbol{x}/\varepsilon)/\varepsilon^d$, where d is the physical dimension. The positions and volumes of the particles are, respectively, $\boldsymbol{x}_p(t)$ and $V_p(t)$. The particles will translate with

the local flow and change volume according to the local fluid dilatation. Using the particle approximations to smooth the singular velocity kernels, we have

$$\frac{\mathrm{d}\boldsymbol{x}_p}{\mathrm{d}t} = \sum_q \boldsymbol{K}_\varepsilon(\boldsymbol{x}_p - \boldsymbol{x}_q) \times \boldsymbol{\Gamma}_q(t) - \sum_q Q_q(t)\boldsymbol{K}_\varepsilon(\boldsymbol{x}_p - \boldsymbol{x}_q), \tag{2}$$

$$\frac{\mathrm{d}V_p}{\mathrm{d}t} = Q_p, \tag{3}$$

where $\boldsymbol{K}_\varepsilon = \boldsymbol{K} \star \zeta_\varepsilon$ is the smoothed velocity kernel. From hereon the flow will be assumed to be two dimensional, so the vorticity has only a single component. Accounting for the radial symmetry of the blob function, we obtain $\boldsymbol{K}_\varepsilon(\boldsymbol{x}) = -\boldsymbol{x}/(2\pi|\boldsymbol{x}|^2)q(|\boldsymbol{x}|/\varepsilon)$, where $q(r) \equiv 2\pi\int_0^r \tau\zeta(\tau)\,\mathrm{d}\tau$. In the method presented here we use an eighth-order-accurate function.

2.1. Equations of motion

Particles also carry enthalpy h, entropy s and density ρ. The particle strengths evolve according to the compressible equations of motion, written as follows:

$$\frac{D\boldsymbol{\omega}}{Dt} = -\boldsymbol{\omega}\theta + \boldsymbol{\omega}\cdot\nabla\boldsymbol{u} + \nabla\times\boldsymbol{F}, \qquad \boldsymbol{F} \equiv h\nabla s + \frac{1}{Re}\frac{1}{\rho}\left(\frac{4}{3}\nabla\theta - \nabla\times\boldsymbol{\omega}\right), \tag{4}$$

$$\frac{D\theta}{Dt} = -\nabla^2 h - \nabla\boldsymbol{u} : (\nabla\boldsymbol{u})^T + \nabla\cdot\boldsymbol{F}, \tag{5}$$

$$\frac{D\rho}{Dt} = -\rho\theta, \tag{6}$$

$$\frac{Ds}{Dt} = \frac{1}{Re}\frac{\Phi}{\rho h} + \frac{1}{RePr}\frac{1}{\rho h}\nabla^2 h, \qquad \Phi = |\boldsymbol{\omega}|^2 + 2\nabla\boldsymbol{u} : (\nabla\boldsymbol{u})^T - \tfrac{2}{3}\theta^2, \tag{7}$$

$$\frac{Dh}{Dt} = -a^2\theta + \frac{\gamma}{Re}\frac{\Phi}{\rho} + \frac{\gamma}{RePr}\frac{1}{\rho}\nabla^2 h. \tag{8}$$

The first two are formed from the curl and divergence of the full Navier–Stokes equations. An acoustic scaling has been used to nondimensionalize the variables in terms of the ambient speed of sound a_∞ and density, ρ_∞; the dynamic viscosity μ; the thermal conductivity k; the specific heat at constant pressure c_p; and a characteristic length scale L. The Reynolds number is $Re = \rho_\infty a_\infty L/\mu$ and the Prandtl number is $Pr = \mu c_p/k$. The fluid properties have been assumed constant and uniform, and the medium to behave as a calorically perfect gas. Thus the local speed of sound satisfies $a^2 = (\gamma - 1)h$, where γ is the ratio of specific heats (taken to be 1.4).

The spatial derivatives in equations (4)–(8) (for all except the velocity) are discretized using PSE [10], extendable to general differential operators as shown by Eldredge *et al* [11]. The essence of the method is the approximation of the derivative D^β (where β is a multi-index denoting the degree of derivative) by the operator,

$$D^\beta f(\boldsymbol{x}_p) \approx \frac{1}{\varepsilon^{|\beta|}}\sum_q V_q(f_q \mp f_p)\eta_\varepsilon^\beta(\boldsymbol{x}_p - \boldsymbol{x}_q), \tag{9}$$

whose kernel, η, is tailored to β with some order of accuracy. For conservation, the choice of sign in (9) is determined by whether the derivative is even or odd.

For spatial derivatives in the velocity, the gradient operator is applied directly to the velocity kernels on the right-hand side of (2). Material derivatives in the continuous equations are replaced by ordinary time derivatives of the particle strengths. The particle forms of equations (4) and (5) are reformulated in terms of particle circulation, Γ_p, and source strength, Q_p, through the use of (3). Equations (2), (3) and the particle forms of (7) and (8) are also

solved. A Greengard–Rokhlin [12] fast summation is used for computing the velocity and its gradient. This approach is extended to the dilating particles by regarding the particles as vortex–source superpositions. Given the initial density of a particle, the density at subsequent times is calculated through $\rho_p(t) = \rho_p(0)V_p(0)/V_p(t)$. This treatment explicitly ensures that the method conserves mass. The particle evolution equations may be solved simultaneously using a standard time integration scheme, such as the fourth-order Runge–Kutta method.

Often it may be sufficient to set the initial dilatation and entropy to zero (unless the circumstances of a particular problem require otherwise) and then compute the initial enthalpy from the initial vorticity (or velocity, rather) through a solution of the following Poisson problem:

$$\nabla^2 h = -\nabla \boldsymbol{u}_s : (\nabla \boldsymbol{u}_s)^T. \tag{10}$$

This effectively reduces the magnitude of the transient that results from not specifying these initial conditions in an exactly consistent manner. With the initial enthalpy and entropy of a particle specified, the initial particle density follows. The particles are initially located on a uniform Cartesian grid, with $V_p(0) = \Delta x^2$, where Δx is the particle spacing.

2.2. Other aspects

Because compressible flows inherently contain radiating components, some means must be provided for absorbing outgoing waves. We enforce the Engquist–Majda condition [13]

$$\left(\frac{\partial h}{\partial t} + \frac{\partial h}{\partial r} + \frac{h}{2r}\right)_{r=R} = 0, \tag{11}$$

on the enthalpy in a circular boundary zone of a few particles' depth at $r = R$. The spatial derivative is approximated by a one-sided form of PSE to respect the boundary [11].

As in incompressible methods, occasional reinitialization of the particles is necessary for the long-term stability of the method. Interpolation of the enthalpy onto the new grid of particles introduces error that is subsequently amplified by PSE and can overwhelm the dilatation through the first two right-hand side terms of (5), which are typically nearly balanced. Through experience we have found that an interpolation kernel with a certain degree of smoothing is necessary to control this error. We use the third-order kernel $W(x_1, x_2) = \frac{1}{\pi}(\frac{15}{8} - \frac{5}{2}x_1^2 + \frac{1}{2}x_1^4)(\frac{15}{8} - \frac{5}{2}x_2^2 + \frac{1}{2}x_2^4)\exp[-(x_1^2 + x_2^2)]$.

3. Spectral character of PSE

In the present method PSE is used in contexts where wave convection is important. It is thus interesting to evaluate the dispersive character of PSE. Consider the linear convection equation $\partial f/\partial t - \partial f/\partial x = 0$. This equation is satisfied by a travelling wave, $\exp[\mathrm{i}(kx - \omega t)]$, for which the frequency is related to the wavenumber by $\omega(k) = k$, indicating that it travels to the right at unit speed, regardless of the wavenumber. If the spatial derivative is approximated by a PSE operator, the wavenumber is effectively modified as follows:

$$k_{mod}(k) = -\frac{\mathrm{i}}{\varepsilon}\tilde{\eta}^{(1)}(k), \tag{12}$$

where $\tilde{\eta}^{(2)}$ is the discrete Fourier transform of the kernel,

$$\tilde{\eta}(k) = \frac{\Delta x}{\varepsilon}\sum_{p=-\infty}^{\infty} \exp(\mathrm{i}kp\Delta x)\eta^{(2)}(p\Delta x/\varepsilon)$$

and Δx is the inter-particle spacing on a stationary grid.

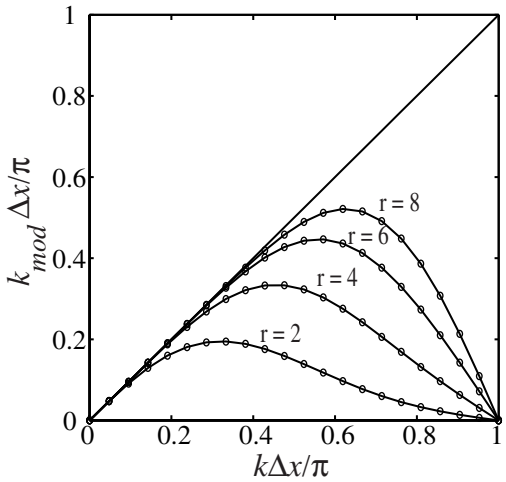

Figure 1. PSE-modified wavenumber of the convection equation, with second-, fourth-, sixth- and eighth-order kernels, $\varepsilon/\Delta x = 1.4$. Exact: '——'; discrete PSE: '—○—'.

Figure 1 depicts the modified wavenumber—computed numerically—for the discrete PSE operator using kernels of various orders of accuracy. By the Nyquist sampling theorem, the maximum wavenumber we can resolve on this grid is $\pi/\Delta x$. The local slope of the modified wavenumber is the group velocity, for which a dependence on k indicates that packets of waves will become dispersed. For the second-order-accurate kernel, the group velocity, $\mathrm{d}k_{mod}/\mathrm{d}k$, strays from unity even for small wavenumbers. However, increasing the order of accuracy of the PSE kernel has a considerable effect on its approximating ability. The eighth-order-accurate PSE scheme is much less dispersive.

Note that the use of the modified relationship between frequency and wavenumber to assess the error of PSE need not be limited to hyperbolic problems. The analysis is equally important in a diffusive context, revealing the extent to which numerical viscosity affects the spectral components.

4. Results and discussion

4.1. Co-rotating vortex pair

The method was applied to a pair of identical vortices in a compressible medium. As the vortices orbit each other they generate sound at a frequency of twice their rotation rate. The problem has been simulated by Mitchell *et al* [14] using a compact finite-difference method on a stretched grid. The vortices are initially placed at $(x, y) = (0, \pm R)$. All quantities are scaled by R and the ambient speed of sound a_∞. For comparison with [14], each vortex is Gaussian-distributed according to

$$\omega = \frac{1.25\Gamma_0}{\pi r_0^2} \exp(-1.25r^2/r_0^2), \tag{13}$$

where the circulation and radius of each vortex are $\Gamma_0 = -2\pi(0.7)^{-1}M_0 r_0$ and $r_0 = 0.15$, respectively. The circulation Reynolds number, $Re \equiv |\Gamma_0|/\nu$ is 7500, the vortex Mach number, $M_0 \equiv U_0/a_\infty$ (where U_0 is the maximum azimuthal velocity of a single Gaussian vortex) is 0.56 and the Prandtl number is 0.7. With these flow parameters, the initial rotation time is $\tau = 105$

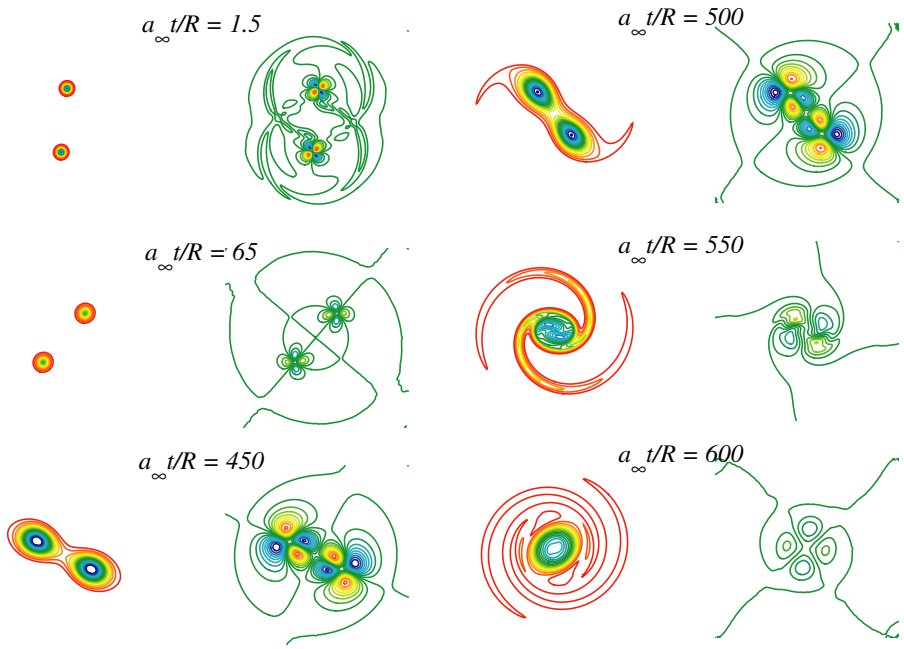

Figure 2. Vorticity (columns 1 and 3) and dilatation (2 and 4) of vortex pair.

and the wavelength of sound is $\lambda = 52.5$. The present investigation focuses on the near-field dynamics and a portion of the acoustic field, from which the far acoustic field is computed exactly using a Kirchhoff surface.

Initially, the flow is taken as homentropic and dilatation free. The initial enthalpy is deduced from a solution of the Poisson equation (10). The particles are distributed on a Cartesian grid inside a circular domain of radius four with 13 particles laid across the diameter of each vortex (approximately 83 500 particles); a boundary zone with a depth of four particles surrounds the domain. The particles are remapped to the same Cartesian grid every two time steps. A fourth-order Runge–Kutta scheme is used for time advancement with a time-step size of $\Delta t = 0.009$. The blob radius and particle spacing are related by $\varepsilon = \Delta x^{0.85}$. All of the kernels used in the interior are eighth-order accurate, except for the one-sided boundary kernel $\eta^{L,(1,0)}$, which is second-order accurate.

The results of the vorticity and dilatation fields are depicted in figure 2. The first set of panels shows the fields soon after the initialization. An acoustic transient is emitted from each core as the dilatation settles to the correct value; the transient is not strong and exits the domain without significant reflection. A quadrupole structure is observed in the dilatation in the next set of panels. The configurations of both fields persist for several rotations, though both quantities are diffused by viscosity over this duration, as observed in the third set of panels (in which the contour levels have been adjusted for better resolution of the diffused magnitudes). After approximately four rotations the continual effects of viscosity and compressibility force the cores to merge, as depicted in the final three sets of panels. The resulting dilatation field is a much weaker quadrupole centred at the core of the new elliptical vortex. Further computation, not shown, reveals the axisymmetrization of the core and thus the disappearance of the dilatation.

The pressure fluctuations observed at one half-wavelength from the origin (on the y-axis), using both a Kirchhoff surface at $R_s = 3.5$ and the Möhring formula [7] are depicted in figure 3 and compared with the results of [14]. Note that because of the symmetry of the problem each rotation of the vortices corresponds to two wavelengths of sound. The magnitude and phase of

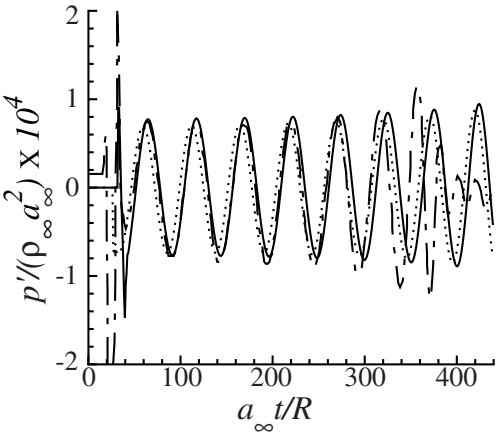

Figure 3. Pressure fluctuations observed at $(0, \frac{1}{2}\lambda)$ from vortex pair. [14]: '–·–'; DVPM and Kirchhoff surface: '——'; DVPM and Möhring analogy: '· · · · · ·'.

the pressure agree quite well for the first two rotations. The large spike in the data of [14] at the outset is due to the acoustic transient. Such a spike is not exhibited in the present results because of the filtering by the Möhring integral and the neglect of the initial transient period for the Kirchhoff surface. After a little more than three rotations the vortices of [14] merge, reflected by a small rise and then quick decay of the pressure. Merger in the present simulation occurs after approximately 5.5 rotations, though. As shown by Melander *et al* [15], incompressible viscous vortices that are initially separated by more than the critical distance for convective merger persist in a 'metastable' state for a duration dependent upon a viscous timescale. The vortices eventually undergo convective merger, but the time at which this begins is quite sensitive to small perturbations. Thus, it is not surprising that merger occurs at a different time in our simulation.

4.2. Leapfrogging vortices

We demonstrate here the application of the DVPM to the slightly more complex problem of two leapfrogging vortex pairs with symmetry about the x-axis. The distribution of the vorticity in each vortex is given by (13). The circulation Reynolds number is 10^5 and the same particle and time-step size are used as in the previous example. Clearly, the forward motion of the leapfrogging vortex system is not a problem for a Lagrangian numerical method. However, in the interest of capturing the acoustic field without the complexity of a moving Kirchhoff surface, we subtract a uniform velocity from each particle to cancel the mean motion. For this mean speed we numerically compute the motion of four point vortices of the same strength and initial configuration, from which the result is $U_{avg} = 0.108$. Using this same point vortex model, we calculate the period of the leapfrogging motion to be $\tau = 72.3$.

We set $r_0 = 0.45$ and $M_0 = 0.1867$. The resulting vorticity and dilatation of the DVPM simulation are depicted in figure 4. The large cores lead to significant overlap between the straining fields of like-sign vortices. They are quickly drawn together as they rotate, shearing each other and coalescing within one-half rotation. During this process, filaments of small vorticity are ejected by each vortex, most of which are stretched and wrap around the vortex cores as they merge. The remainder of the filaments are not pulled with the structures but leave the left-hand side of the domain (or, in a fixed frame, remain stationary while the vortical structures advect forward). The merging cores eventually form two elliptical vortices. The

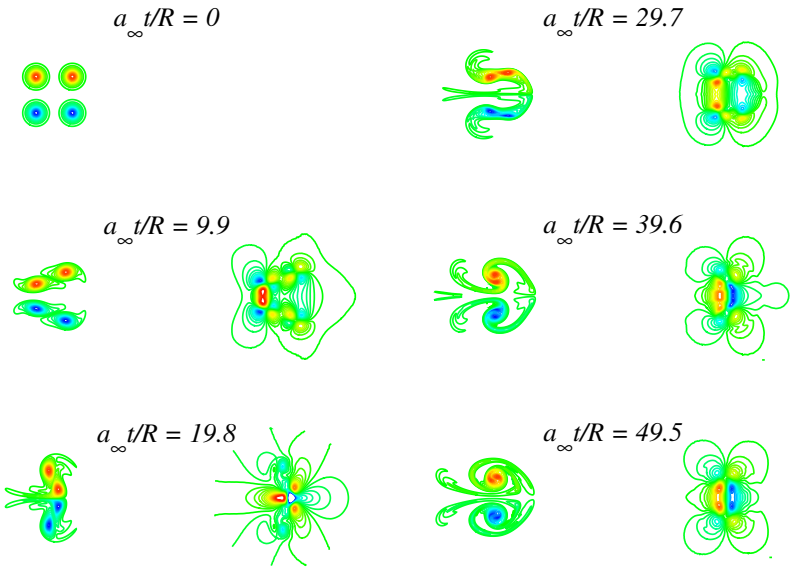

Figure 4. Vorticity and dilatation of leapfrogging vortices.

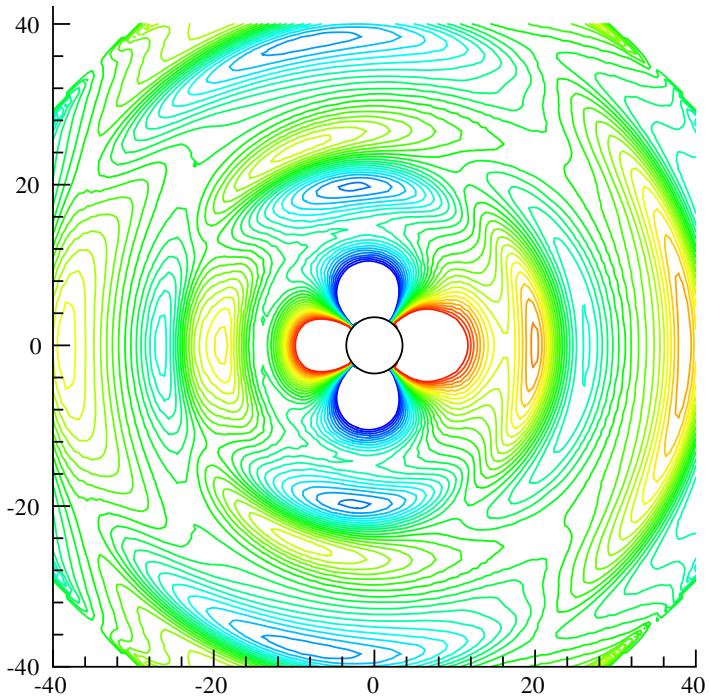

Figure 5. Acoustic field of leapfrogging vortices at $a_\infty t/R = 60$.

dilatation during the merging process transforms from four quadrupole structures that advect with each distinct core, into two relatively stationary quadrupoles in the elliptical state.

The sound radiated by this process is computed using a Kirchhoff surface at $R_s = 3.5$. The acoustic field at $t = 60$ is depicted in figure 5, with the Kirchhoff surface depicted by a circle at the origin. Note that the observation points are moving in the same frame as the vortex system,

but the very slight forward motion leads to very little Döppler effect. The acoustic nearfield exhibits a quadrupole structure, which translates into a cylindrical wave pattern in the farfield. These cylindrical waves are approximately divided into four quadrants: two above and below the vortex system, and two ahead and behind it. They do not possess a fore/aft symmetry. The quadrant ahead of the system comprises a larger sector of the circle than the one behind. This directivity is due to a slight rearward shifting of the nearfield quadrupole by the dipole velocity field of the vortices.

5. Conclusions

A vortex particle method for two-dimensional compressible flow has been developed. While previous particle methods have incorporated the effects of compressibility, this method is the first that solves the full compressible Navier–Stokes equations. One advantage of the vorticity-based approach is that incompressible flows can be solved by simply 'flipping a switch', as no special consideration must be given to enforcing conservation of mass. Because of the small relative magnitude of the acoustic field, the method requires more delicate application of techniques that have proven robust for incompressible vortex methods, for instance computation of derivatives using PSE (which must now suppress dispersion of waves) and interpolation during remeshing (which must preserve smoothness in the interpolated quantities).

Further developments are necessary in order to solve problems of larger scale. A more 'efficient' definition of the particles—for instance, a division of the particles into those that are active and those that are passive in the velocity induction—is currently being explored. Along the same lines, an implementation of the method with variably sized particles, which would allow more efficient resolution of flows with disparate length scales, is under development. Such an extension would make simultaneous solution of the near and acoustic fields practical. The boundary treatment proposed here is sufficient for absorbing incident acoustic waves, but does not fully exploit the decomposition of the velocity at the heart of the method. A more natural scheme is currently being developed. Finally, using existing techniques for computing vortex stretching, the method is readily extendable to three-dimensional flows.

JoT 3 (2002) 036

Acknowledgments

The first author gratefully acknowledges support from a Graduate Research Fellowship from the National Science Foundation. This research was supported, in part, by the National Science Foundation under Grant No 9501349.

References

[1] Cottet G-H and Koumoutsakos P 2000 *Vortex Methods: Theory and Practice* (Cambridge: Cambridge University Press)
[2] Gingold R A and Monaghan J J 1977 Smoothed particle hydrodynamics: theory and application to non spherical stars *Mon. Not. R. Astron. Soc.* **181** 375–89
[3] Anderson C R 1985 A vortex method for flows with slight density variations *J. Comput. Phys.* **61** 417–44
[4] Krishnan A and Ghoniem A F 1992 Simulation of rollup and mixing in Rayleigh–Taylor flow using the transport-element method *J. Comput. Phys.* **99** 1–27
[5] Ghoniem A F, Chorin A J and Oppenheim A K 1982 Numerical modelling of turbulent flow in a combustion tunnel *Phil. Trans. R. Soc.* A **304** 303–25
[6] Quackenbush T R, Boschitsch A H, Winckelmans G S and Leonard A 1996 Fast Lagrangian analysis of three dimensional unsteady reacting flow with heat release *AIAA Paper* 96-0815
[7] Möhring W 1978 On vortex sound at low Mach number *J. Fluid Mech.* **85** 685–91

[8] Knio O M, Collorec L and Juvé D 1995 Numerical study of sound emission by 2D regular and chaotic vortex configurations *J. Comput. Phys.* **116** 226–46
[9] Pothou K P, Voutsinas S G, Huberson S G and Knio O M 1996 Application of 3-d particle method to the prediction of aerodynamic sound *Vortex Flows and Related Numerical Methods II* (*ESAIM vol 1*)
[10] Degond P and Mas-Gallic S 1989 The weighted particle method for convection-diffusion equations, Part 1: the case of an isotropic viscosity *Math. Comput.* **53** 485–507
[11] Eldredge J D, Leonard A and Colonius T 2002 A general deterministic treatment of derivatives in particle methods *J. Comput. Phys.* **180** 686–709
[12] Greengard L and Rokhlin V 1987 A fast algorithm for particle simulations *J. Comput. Phys.* **73** 325–48
[13] Engquist B and Majda A 1977 Absorbing boundary conditions for the numerical simulation of waves *Math. Comput.* **31** 629–51
[14] Mitchell B E, Lele S K and Moin P 1995 Direct computation of the sound from a compressible co-rotating vortex pair *J. Fluid Mech.* **285** 181–202
[15] Melander M V, Zabusky N J and McWilliams J C 1988 Symmetric vortex merger in two dimensions: causes and conditions *J. Fluid Mech.* **195** 303–40